Thermal properties of the barium nitrate - metallic fuel (aluminum, magnesium and magnalium) systems

Yuriy Verbovytskyy

GRS, Green Street, 79000, Lviv, Ukraine, xyuriyfly@gmail.com

Abstract: *This study utilized X-ray diffraction to characterize the phase composition of the product obtained by the oxidation and combustion of aluminum, magnesium, and magnalium powders, as well as their stoichiometric mixtures with barium nitrate. Magnesium is a highly reactive metal, readily burning and oxidizing both as a pure powder and when mixed with barium nitrate. In contrast, even powdered aluminum exhibits greater resistance to oxidation. The observation of a two-stage oxidation behavior in both magnalium and its barium nitrate mixture sheds light on the potentially complex combustion mechanisms at play in strobe pyrotechnics. Stoichiometric $Ba(NO_3)_2$/AlMg exhibits poor ignitability, unstable combustion, and self-extinguishing tendencies. Catalysts, like bismuth oxide, significantly alter these burning characteristics.*

Keywords: *Pyrotechnic strobe, Magnalium, Oxidation behavior, Combustion products.*

Introduction

High-energy processes involving inorganic nitrates are widely used for the synthesis of ceramic materials and for obtaining various pyrotechnic effects. Mixtures based on barium nitrate with magnalium (a powdered Al-Mg alloy), which are widely used to create classic white strobe mixtures, have not yet been sufficiently studied. The practical compositions of such mixtures may also contain small amounts of one or more additional oxidizers (potassium nitrate, potassium chlorate, potassium perchlorate, ammonium perchlorate), additional fuel (sulfur, metal sulfides), a binder (nitrocellulose, dextrin) and a catalyst (copper compounds) [1].

The nature of combustion of such mixtures is a subject of debate in scientific groups and among amateurs. It is believed that the combustion process of strobe compositions includes two stages: a dark, or smolder phase – a relatively slow and low-temperature combustion that emits little or no light, and a bright, or flash phase – a fast and highly exothermic reaction that reaches a high temperature and emits a bright flash of visible light [2]. Examples of such reactions are proposed by Jennings-White [3]. The best way to determine the processes that occur in these, or other, reactions would be to analyze the nature of the prepared layers before combustion, the products that form in layers while they are burning and the final products of combustion. Ideally, these measurements should be made in real time, using some in situ method. For the study of fast pyrotechnic processes, high-speed video recording and various spectral analyses are widely used, which make it possible to identify sources of radiation and the intensity of the emitted light in successive short intervals of time. X-ray diffraction (XRD) and microscopic analyses (MA) are often used to establish the phase composition of intermediate combustion processes (the process is stopped, the products are cooled) and the final combustion products (the process is allowed to complete, the products are cooled). Here we speculatively assert that the obtained phase composition corresponds to that which took place in the real combustion process. High temperature XRD, differential thermal and thermogravimetric analyses (DTA and TGA) are important methods of studying the individual components and their mixtures, in

Article Details | ***Article No:- 0124***

Manuscript Received:- 24/01/2024 | ***Final Revisions:- 28/02/2024***

Publication Date:- 28/02/2024 | ***Archive Reference:- 2148***

which the components are heated to temperatures up to 1200°C, at a constant rate of up to 20°C per minute [4]. Phase-structural changes of crystalline substances, including polymorphic transformations, decomposition of substances or formation of new ones, can be seen by using in-situ XRD analysis. Thermal (exothermic and endothermic) effects, such as melting, evaporation, decomposition and formation of new substances, can be observed with the help of DTA. During TGA analysis, a change in the weight of the examined samples, as a result of processes such as decomposition or oxidation, can be recorded. Usually, the time intervals of such studies are much longer than the combustion process, but they provide some information about the changes that can take place in that part of the pyrotechnic sample that is heated to a certain temperature before ignition.

A strobe pyrotechnic composition is, usually, a multi-component mixture, and in order to better understand the processes that take place during its combustion, one should first know the properties of its individual components and binary mixtures of oxidizer and fuel. As mentioned above, a simple representative of this type of composition the one based on barium nitrate with magnalium. In the literature, in journals such as *Propellants, Explosives, Pyrotechnics, Thermochimica Acta, Combustion and Flame,* and *Combustion, Explosion and Shock Waves*, one can find many works devoted to the study of the oxidation, combustion, and the corrosion or aging products of magnesium, aluminum and magnalium, and the processes accompanying them. It is beyond the scope of this work to mention them all, so the citation of individual works will be made in the section on the results of the experiment. Few works [5-17] have been devoted to the study of binary and multicomponent mixtures comprising nitrates of alkaline earth metals and metal powders (Al, Mg, Al-Mg alloys).

In this work, based mainly on the results of X-ray phase and structural analysis, we show the phase-structural changes of individual components and initial mixtures based on barium nitrate and an active metal under the conditions of their intermediate and final oxidation, and the phase composition of their combustion products.

Experimental

Commercial powders from several manufacturers were used in the work. Magnesium and aluminum were powders of 325 mesh, spheroid <0.04 mm, <0.08 mm and flakes 0.2 - 0.5 μm with a purity of 98-99%. Magnalium (1:1) was purchased in the form of pieces several centimeters in size; it was ground and sieved to obtain a fraction with particle sizes between 0.04 and 0.08 mm. Some Al-Mg alloys were prepared by melting compact pure metals in an inert atmosphere. The mixtures that did not contain a binder were pressed in the form of tablets 6-8 mm in diameter to 90-95% of the theoretical maximum density (TMD). Metal powders and samples of the pressed tablets were placed in corundum crucibles and heated in air at temperatures of 400, 650 or 850°C for times that ranged from a few minutes to several days. Rods of the compositions that included a binder were made by using the cut star method. The surface of those rods that stopped burning after at least one flash was cut with a scalpel for further studies. In the case of rods that burned to completion, the ash and their smoke – which was captured by a special device – were collected for further analysis.

The purity of the selected components and starting mixtures was checked by X-ray fluorescence methods. The metal powders, and the surface and fractures of selected reacted tablets were observed by means of an electron microscope (Hitachi S-2400). Combustion reaction products and sections of pre-reacted (pre-heated) tablets were ground into powder for subsequent analyses. X-ray phase and structural analysis was performed on a PANalytical X'Pert Pro (CuKα-radiation) diffractometer. Theoretical diffraction data were generated based on open data from The Materials Project website [18] by using the Powder Cell program [19]. The selected patterns were refined by the full-profile method using the FullProf program [20]. In the figures of X-ray diffraction patterns, the values of the profile factor, R_p, and the weighted profile factor, R_{wp}, indicate the reliability of the fit between the proposed model and the observational data. Lower values indicate a better fit. Their definitions are: $R_p = \Sigma |y_i - y_{c,i}| / \Sigma |y_i|$ and $R_{wp} = (\Sigma w_i \cdot (y_i -$

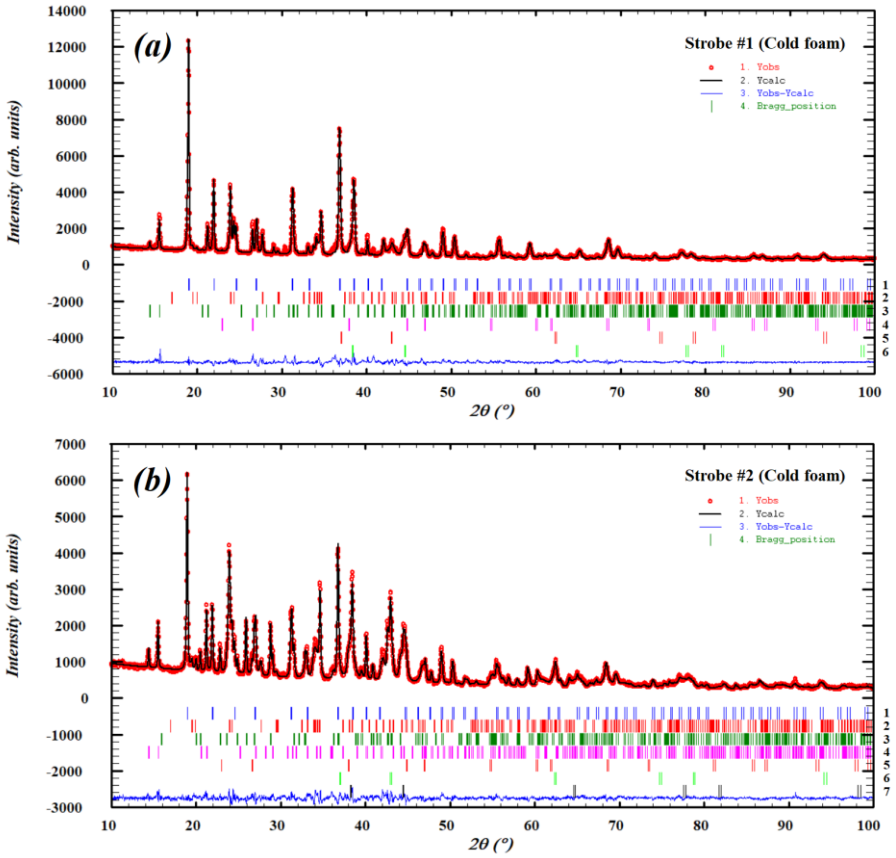

Figure 1. Refined powder X-ray diffraction patterns for the cold foams: (*a*) composition #1 (1 - $Ba(NO_3)_2$, 2 - $BaCO_3$, 3 - $K_2Ba(NO_2)_4$, 4 - KNO_2, 5 - MgO, 6 - Al; R_p = 5.73%, R_{wp} = 7.98%) and (*b*) composition #2 (1 - $Ba(NO_3)_2$, 2 - $BaCO_3$, 3 - $BaSO_4$, 4 - $K_2Ba(NO_2)_4$, 5 - KNO_2, 6 - MgO, 7 - Al; R_p = 4.57%, R_{wp} = 5.79%).

$y_{c,i})^2 / \Sigma w_i \cdot y_i^2)^{(1/2)}$, where y_i and $y_{c,i}$ are the experimental and calculated intensity of diffraction reflections at the i^{th} step, and w_i is the weighting scheme. In a standard X-ray powder diffraction pattern $w_i = 1 / y_i$.

DTA/TGA analysis was performed for comparison with literature data.

Results and Discussion

During strobe combustion, particularly when using the high-speed video recording method, or on strobes with a low flash frequency, the following processes were observed. After ignition, the relatively flat surface of the strobe starts to smolder, with a steady increase in the size of the smoldering region, whose surface turns into a mobile foam from which gases escape in places. The amount of such foam increases, especially in unjacketed samples or on samples with a large diameter, and its temperature increases. In strobes with a low flash frequency, the author observed a change in the color of the surface of the foam, before the flash occurred, from a clearly visible red to a light, bright yellow. Finally, the moment comes when a flash occurs, resulting in a short interval with high temperature and maximum light emission, almost completely consuming the foam. The heat released during the flash warms the next layer of the mixture, which begins to smolder, and the process is repeated.

Phase analysis of the cold foam from white strobes

At the beginning of the research, different white strobe compositions, similar in composition and behavior to those described in an earlier study [21] of mixtures that only differed by the inclusion of small amounts of additional materials, were combusted. When there was a chance of extinction after the flash, we cut the cold foam with a scalpel and analyzed its phase composition. The foam was gray in color, porous in structure and had an increased volume and rounded shape. Figure 1 presents refined diffractograms of the cold foams. Table 1 lists the initial constituents of the compositions, and the materials present in both the prepared pellets and the cold foam, as identified by X-ray phase analysis. We found that, during the preparation of the

Table 1. The composition of the strobes, their phase analysis after grinding and mixing the components, and analysis of the cold foam section of the extinguished strobe

No.	Initial composition	Phase content of the prepared strobes	Phase content of the cold foam
1.	$Ba(NO_3)_2$ – 63% KNO_3 – 9% AlMg – 28% NC – 3% (additional)	$Ba(NO_3)_2$ – 60% KNO_3 – 7% $K_2Ba(NO_3)_4$ – 5% AlMg – 28%	$Ba(NO_3)_2$ $BaCO_3$ KNO_2 $K_2Ba(NO_2)_4$ MgO Al Unknown compounds
2.	$Ba(NO_3)_2$ – 63% KNO_3 – 9% AlMg – 25% S – 3% NC – 3% (additional)	$Ba(NO_3)_2$ – 59% KNO_3 – 6% $K_2Ba(NO_3)_4$ – 7% AlMg – 25% S – 3%	$Ba(NO_3)_2$ $BaCO_3$ $BaSO_4$ $K_2Ba(NO_2)_4$ KNO_2 MgO Al Unknown compounds

samples, barium nitrate and potassium nitrate partially interacted to form the double salt, $K_2Ba(NO_3)_4$. In the cold foam we found the nitrite, $K_2Ba(NO_2)_4$, the result of the partial decomposition of the double nitrate of potassium and barium. Potassium nitrate decomposed to potassium nitrite as expected. Barium nitrate decomposed to the oxide, which, interacting with atmospheric CO_2 during the preparation of the mixture for analysis, formed $BaCO_3$. The presence of MgO and elemental Al may suggest that the magnalium was selectively oxidized in the foam, but we could not exclude the partial oxidation of aluminum to amorphous Al_2O_3, which cannot be identified by the X-ray method. The foam of the strobe composition that contained sulfur showed the presence of barium sulfate, the result of the interaction of barium nitrate and sulfur during the dark phase. On the diffractograms of the foam in both cases, we found also reflections of low intensity (I/Imax < 5%), that we could not identify. In the first case, these reflections were at 2θ angles of: 15.06, 27.51, 30.38, 36.29, 37.56, 40.80, 42.50 and 43.48 degrees. In the second case the 2θ angles were: 14.25, 18.38, 27.50, 30.15, 30.40, 36.04 and 37.55 degrees. Perhaps these reflections are evidence of the formation of new, unknown or metastable compounds; it is possible that they were formed when the powdered foam cooled to room temperature, or they could be the result of interactions with carbon dioxide and/or moisture. The content of these compounds in the foam was estimated to be no more than 3-5 wt. %.

The fact of identifying pure aluminum in the foam and the absence of magnalium led to the opinion that the two-stage burning process of strobes based on barium nitrate and magnalium can be due to the selective oxidation of magnesium in the smoldering phase: $Ba(NO_3)_2 + 5Mg = BaO + N_2 + 5MgO$ and energetic oxidation of aluminum in the flash phase: $3Ba(NO_3)_2 + 10Al = 3BaO + 3N_2 + 5Al_2O_3$. For this purpose, we investigated the oxidation at different temperatures of both pure metal powders and their mixtures with barium nitrate. Separately, we conducted a phase analysis of their combustion products.

Barium nitrate and magnalium are necessary components of classic white strobes

Barium nitrate

Barium nitrate is colorless cubic crystals with a density of 3.24 g/cm^3 and a melting point of 592ºC. Above this temperature, barium nitrate decomposes: $2Ba(NO_3)_2 = 2BaO + 4NO_2 + O_2$. This process takes place more intensively with increasing temperature [22]. These findings are in good agreement with our data obtained by DTA/TGA, as shown in Figure 2. We observed two endothermic peaks, the first of which corresponds to the melting of barium nitrate, and the wider second one to

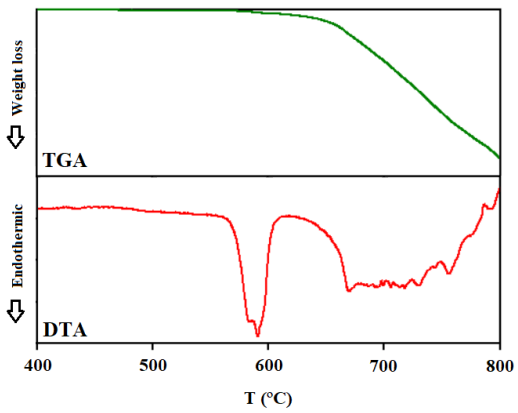

Figure 2. DTA/TGA curves for ball milled barium nitrate at a heating rate of 10°C/min in air.

its decomposition. According to our TGA data, almost 90% of barium nitrate has decomposed by the time the temperature has risen to 800°C. In general, the decomposition process is more complex than indicated by the above equation. It can start at a lower temperature [23-28] and depends on many factors, in particular, the structure of the barium nitrate powder and the presence of impurities and different additives, such as other inorganic salts and catalysts. These facts are important in the development of new strobe mixtures based on barium nitrate. The barium nitrate used in the experiments was ball milled to a fine powder and, according to X-ray diffraction data, did not contain additional impurities. Barium oxide, which was formed during the decomposition of $Ba(NO_3)_2$, turned out to be very reactive and absorbed CO_2, forming barium carbonate.

The binary Al-Mg alloy system

Although magnalium with a 1:1 composition by weight is most often used in pyrotechnics, it will be useful to pay attention to the whole of the Al-Mg phase diagram and the intermetallic compounds (phases) that are formed. According to Murray [29] the system is characterized by three eutectics: $Al_{31}Mg_{69}$ (437°C, L = Mg + γ), $Al_{59}Mg_{41}$ (450°C, L = γ + β) and $Al_{62}Mg_{38}$ (450°C, L = β + Al). Phases γ and β melt congruently at 460 and 451°C and are characterized by homogeneity ranges. The R phase of constant composition exists only between 320 and 370°C. From the crystallographic point of view, all these phases have complex structures [30, 31]. Aluminum and magnesium form limited solid solutions with the limiting compositions of $Al_{81}Mg_{19}$ and

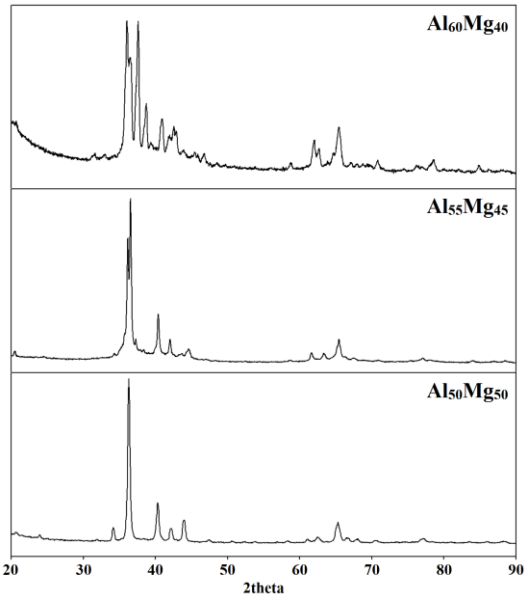

Figure 3. X-ray diffraction patterns of selected as-prepared Al_xMg_y alloys.

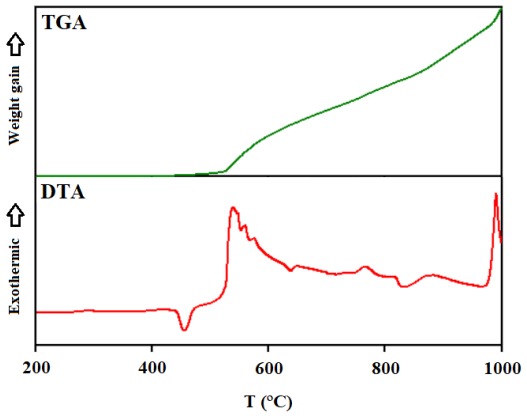

Figure 4. DTA/TGA curves for magnalium at a heating rate of 10°C/min in air.

$Al_{12}Mg_{88}$, respectively. The γ phase, which interests us more, also has a wide homogeneity range of 45-62 at. % Mg. According to the latest works [32, 33], the central part of the Al-Mg state diagram was reconstructed. In the annealed $Al_{50}Mg_{50}$ alloys an intermetallic with a cubic structure is formed; when the aluminum content increases, the structure of the γ-phase becomes more complicated, the authors designate it as γ'. Ball milled, melt-spinning or cast Al-Mg alloys can include various metastable phases as well as quasi-crystals [34-37].

We have synthesized three alloys with three different compositions ($Al_{50}Mg_{50}$, $Al_{55}Mg_{45}$ and $Al_{60}Mg_{40}$), which confirm the formation of the AlMg (γ), $Al_{1+x}Mg_{1-x}$ (γ') and Al_3Mg_2 (β) phases

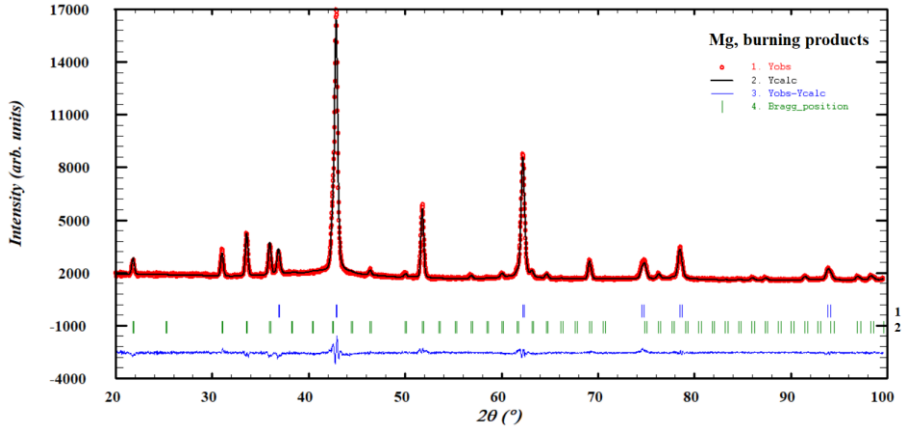

Figure 5. Refined powder X-ray diffraction patterns for the combustion magnesium powder at 850°C (1 - MgO, 2 - Mg_3N_2; R_p = 1.98%, R_{wp} = 2.63%).

in slowly cooled alloys. The corresponding diffraction patterns are presented in Figure 3. In all our further studies, we used only a 1:1 composition alloy.

DTA/TGA curves for magnalium (1:1) with a particle size less than 0.04 mm are presented in Figure 4. According to the literature [38-46], these curves strongly depend on the composition, manufacturing method and dispersion of Al-Mg alloy powders, and the heating atmosphere (air, oxygen, argon). According to our DTA data, we can clearly distinguish three peaks: an endotherm at 455°C, which corresponds to the melting of the Al-Mg alloy, and two exotherms – a broad, compound one with a maximum at 538°C and a sharp one at 991°C. Weak effects of an unknown nature are observed between these temperatures. We assume that the exothermic peaks observed on DTA correspond to the oxidation of the magnesium (or magnesium-rich phase) and residual aluminum, respectively. The TGA evidence indicates that oxidation of the alloy is already occurring at temperatures just above 400°C. Above 527°C, the rate of oxidation increases and up to 1000°C it speeds up or slows down in some places. According to the TGA experiment, almost 80% of magnalium was oxidized at a temperature of 1000°C. However, as is further discussed in a later section, even at that temperature, non-oxidized aluminum was detected by X-ray diffraction.

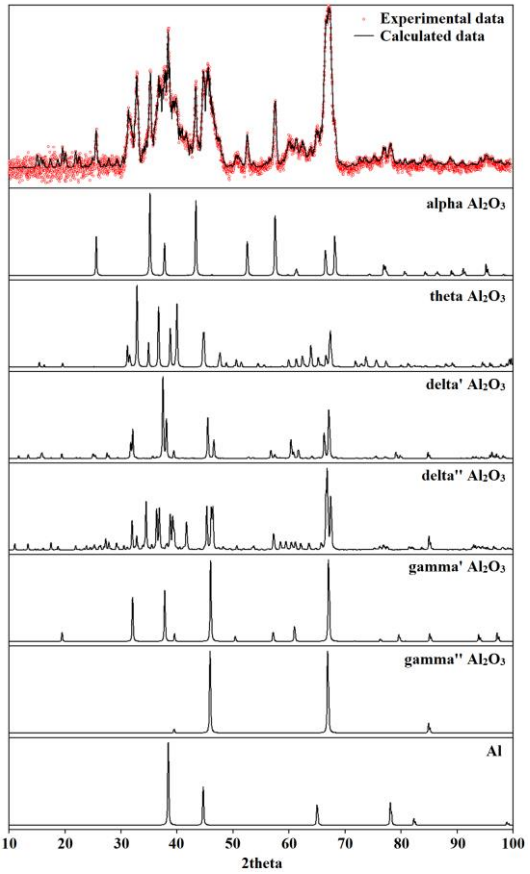

Figure 6. Experimental X-ray diffraction pattern of the oxidation products of aluminum flakes at 850°C, compared with the theoretical patterns for a range of potential products (R_p = 13.4%, R_{wp} = 15.6%).

Phase analysis of oxidation and combustion products of aluminum, magnesium and magnalium

Oxidation and ignition of magnalium, magnesium and aluminum was carried out in air, at temperatures of 400, 650 and 850°C. The selection of these temperatures was based on the following considerations: at 400°C or above, according to the Al-Mg phase

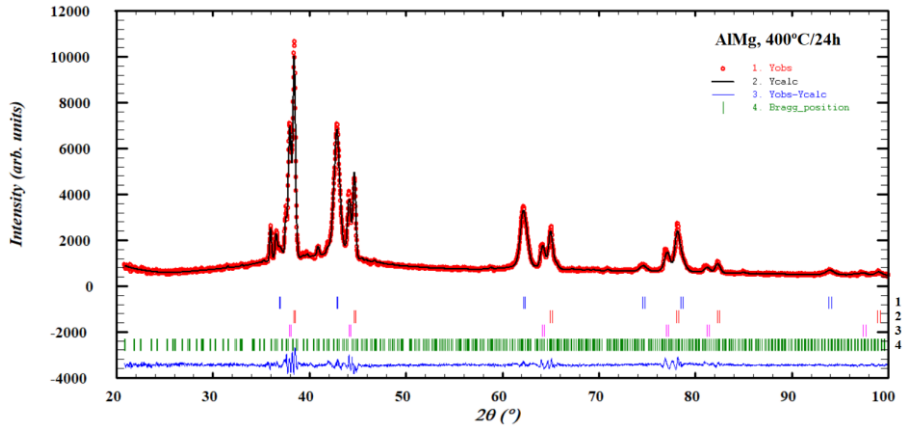

Figure 7. Refined powder X-ray diffraction patterns for the oxidized product of magnalium at 400°C (1 - MgO, 2 - Al, 3 - $Al_{0.85}Mg_{0.15}$, 4 - Al_3Mg_2; R_p = 3.90%, R_{wp} = 5.04%).

diagram, inflow of 1:1 based alloys is possible; at 650°C or above, magnesium and aluminum will be in the liquid state, and it is the temperature at which intensive decomposition of barium nitrate occurs; a temperature of 850°C results in the rapid ignition of metal powders, as well as causing the cooled foam from partially reacted strobe samples to produce a flash. Note that, in this context, the term ignition refers to a process that results in the production of a visible flame, whereas oxidation relates to a slower reactive process that does not result in ignition. In the case of oxidation, we recorded the increase in weight of the samples at certain time intervals and performed X-ray phase analysis. When ignition occurred, the analysis of ash was carried out after the disappearance of the flame.

Oxidation and ignition of magnesium

The oxidation and combustion of magnesium has been studied for decades and it is almost impossible to add any new data to this. We can only confirm the fact that the oxidation of magnesium proceeds quite easily until it is completely converted to MgO. For more information on magnesium oxidation processes, the author recommends several references [47-51]. Magnesium ignited easily at 850°C and turned into a loose, light-yellow powder. As indicated in Figure 5 – and as expected since the combustion took place in air [52] – in addition to magnesium oxide MgO, its nitride, Mg_3N_2, was also identified in the reaction products.

Oxidation and ignition of aluminum

More publications are devoted to the oxidation and combustion of aluminum than to magnesium [53-56]. Due to the dense oxide film, aluminum oxidizes with greater difficulty than magnesium. In addition, aluminum oxide, which is formed and grows during oxidation, undergoes several polymorphic transformations. Today, in addition to the thermodynamically stable Al_2O_3 of a corundum type, about 20 different structures are known, which are usually denoted by letters of the Greek alphabet [57, 58]. Aluminum powders are also more difficult to ignite than magnesium, and the ease of ignition is dependent on their particle shape and size. Aluminum nanopowders have the lowest ignition temperature [59, 60]. The burning of aluminum in air can also be accompanied by the formation of aluminum nitrides or oxonitrides [61, 62]. The study of aluminum oxidation products has been the subject of several theses [63, 64].

We oxidized samples of both spheroid and flake aluminum. In the case of the spherical powder, there was no weight change after 24 hours at 650°C, and only partial melting and a weight gain of 12% was observed after heating for 24 hours at 850°C. The flake powder oxidized faster; the weight gains after 24 hours at 650°C and 850°C were 11% and 69% respectively, the latter value indicating a reaction conversion of 78%. In this sample, the X-ray phase analysis, as shown in Figure 6, indicated that, in addition to pure aluminum, several modifications of aluminum oxide were present.

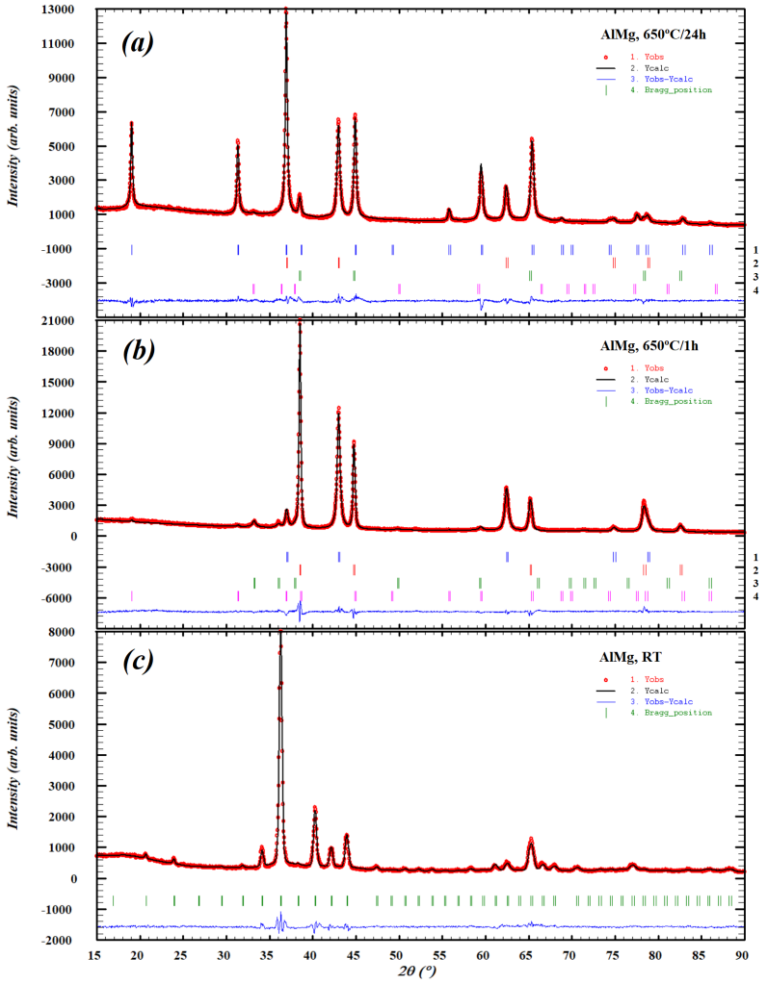

Figure 8. Refined powder X-ray diffraction patterns for magnalium and its oxidation products: (*a*) (1 - $MgAl_2O_4$, 2 - MgO, 3 - Al, 4 - α'-Al_2O_3; R_p = 3.83%, R_{wp} = 5.12%), (*b*) (1 - MgO, 2 - Al, 3 - α'-Al_2O_3, 4 - $MgAl_2O_4$; R_p = 4.36%, R_{wp} = 5.58%), (*c*) (AlMg, R_p = 5.13%, R_{wp} = 6.75%).

Attempts to ignite spheroid aluminum at 850°C were unsuccessful. Although flake aluminum did ignite at this temperature, it tended to self-extinguish. In the products of its reaction only a small amount of one crystalline oxide was found. It can be concluded that rapid oxidation of aluminum and its ignition requires high temperatures.

Oxidation and ignition of magnalium

Oxidation, ignition and combustion of the Al-Mg powders have been studied by a number of authors [38-46]. Our magnalium powder shows a tendency to oxidize, even at the low temperature of 400°C. After an hour the changes were not visible, but after 24 hours we recorded an increase in weight of 22%. In the X-ray diffraction pattern of the resulting powder, shown in Figure 7, an oxidation product, MgO, was already observed. This indicates that the initial composition of magnalium had changed, and among unreacted products Al_3Mg_2 (β phase), $Al_{0.85}Mg_{0.15}$ (solid solution) and pure aluminum were identified.

At 650°C, the oxidation of magnalium is more active; after one hour the weight increased by 31%, and after 24 hours by 67%. The phase-structural changes are well illustrated in Figure 8. The initial magnalium powder has a cubic structure (the γ phase, which is sometimes denoted in the literature as $Mg_{17}Al_{12}$). After one hour, that structure completely disappeared, leaving a mixture whose principal components were pure aluminum and magnesium oxide. The trace amounts of Al_2O_3 and $MgAl_2O_4$ were also detected in this sample. Further heating leads to the oxidation of aluminum, the oxide of which interacts with magnesium oxide, mainly forming the mixed oxide, $MgAl_2O_4$. Assuming the two-stage oxidation of magnalium, the reaction $2AlMg + O_2 = 2Al + 2MgO$ will result in a 31% increase in weight. The agreement of this value with the observed increase in

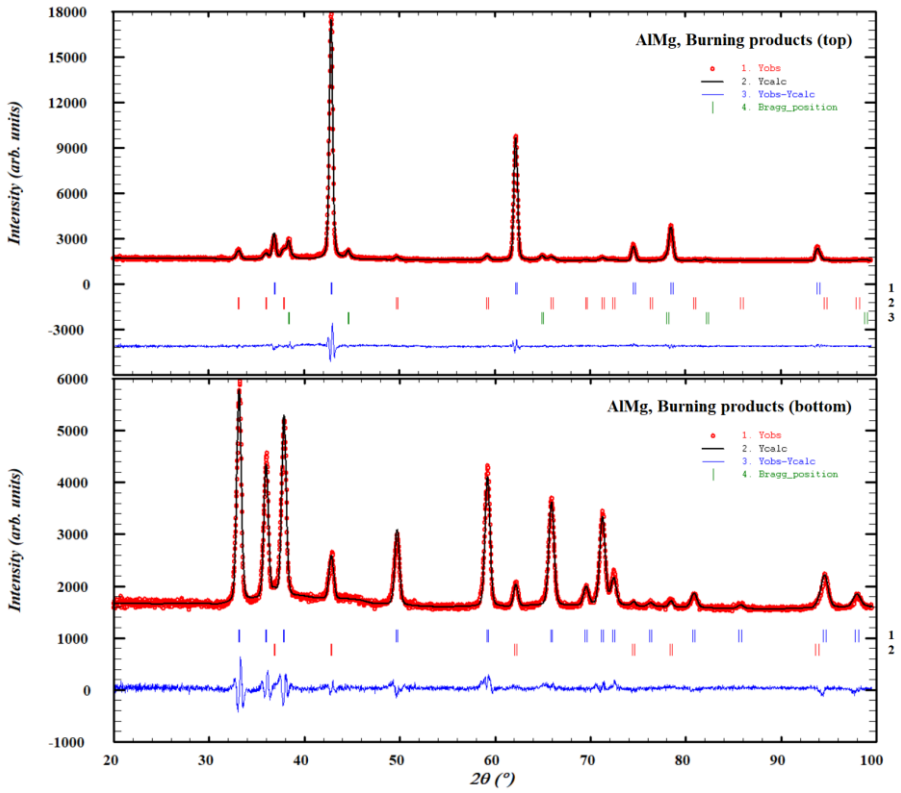

Figure 9. Refined powder X-ray diffraction patterns for the combustion products of magnalium at 850°C: (*a*) (1 - MgO, 2 - AlN, 3 - Al; R_p = 2.14%, R_{wp} = 2.94%) and (*b*) (1 - AlN, 2 - MgO; R_p = 1.90%, R_{wp} = 2.67%).

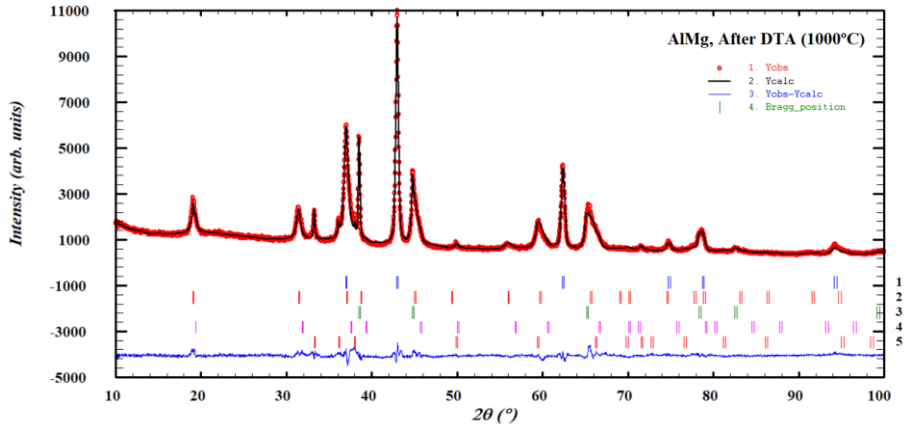

Figure 10. Refined powder X-ray diffraction patterns for the sintered products of magnalium after DTA/TGA up to 1000°C (1 - MgO, 2 - $MgAl_2O_4$, 3 - Al, 4 - γ-Al_2O_3, 5 - α'-Al_2O_3; R_p = 4.43%, R_{wp} = 5.78%).

weight in the first hour indicates that it is, indeed, likely to be the result of the preferential oxidation of the magnesium content of the magnalium, according to the above equation. The overall reaction for the complete oxidation of magnalium, including the oxidation of the aluminum and the interaction between the two oxides, can be written as $4AlMg + 5O_2 = 2Al_2O_3 + 4MgO = 2MgAl_2O_4 + 2MgO$, resulting in a 78.0% increase in weight. The observed increase in weight after heating for 24 hours corresponds to that second reaction being 86% complete at that time.

The burning of magnalium in bulk led to the formation of two visually distinguishable parts: an upper phase, with white to light gray color and a lower phase, with gray to dark gray color. These parts were mechanically separated and analyzed using X-ray phase analysis, with the results as shown in Figure 9. The upper part mostly contained magnesium oxide (MgO), while the lower one consisted mainly of aluminum nitride (AlN). This result can be explained if it is assumed that the combustion of magnalium in air was also a two-stage process: first the magnesium burned to form the oxide, $2AlMg + O_2 = 2Al +$

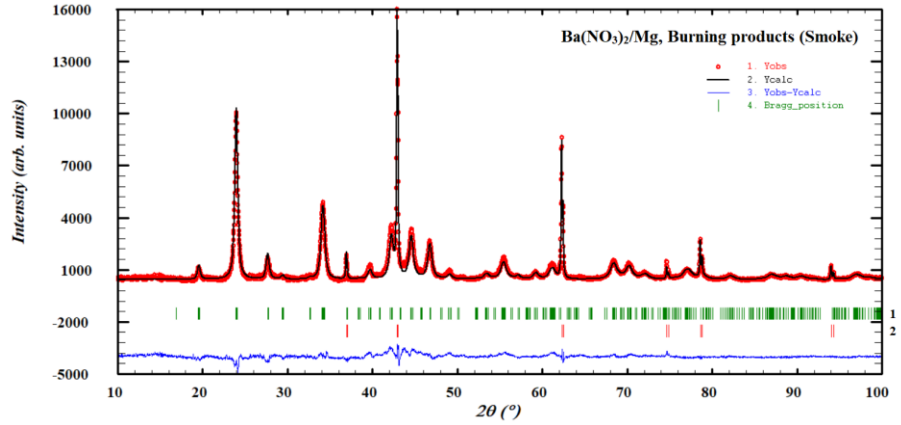

Figure 11. Refined powder X-ray diffraction patterns for the combustion products of $Ba(NO_3)_2$/Mg (1 - $BaCO_3$, 2 - MgO; R_p = 8.60%, R_{wp} = 11.2%).

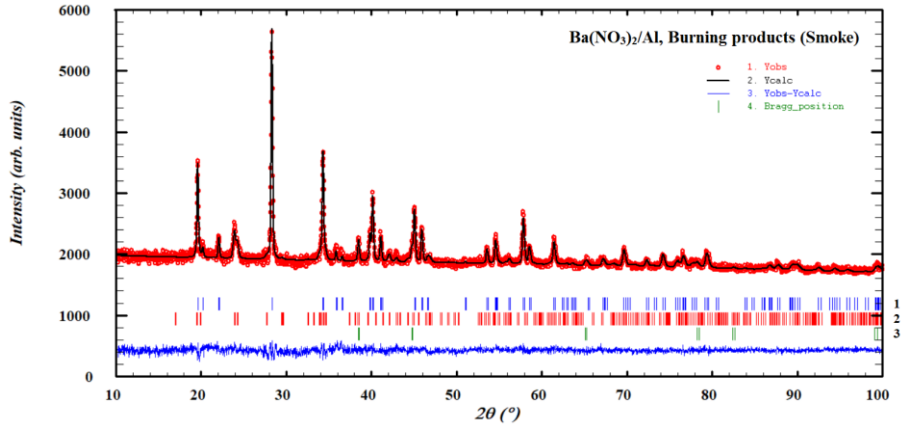

Figure 12. Refined powder X-ray diffraction patterns for the combustion products of $Ba(NO_3)_2$/Al (1 - $BaAl_2O_4$, 2 - $BaCO_3$, 3 - Al; R_p = 1.44%, R_{wp} = 1.88%).

2MgO and then, in the absence or deficit of oxygen, the aluminum reacted with atmospheric nitrogen to form the nitride, 2Al + N_2 = 2AlN. Visually, the reaction initially produced a bright white light, together with white smoke, but then progressed to a less violent burning of the remaining powder at bright red heat.

There exist several studies that discuss the phase composition of the partially and/or completely oxidized products [38, 41, 42, 44, 46]. In several works, the authors observed the two-stage nature of magnalium combustion. Oxidation of magnesium in AlMg is easy and slow, but that of aluminum is more difficult and slower, even when it is in a liquid state. As mentioned above, and illustrated in Figure 10, pure aluminum remained in the sample after DTA/TGA runs in which the sample was heated to 1000°C.

Phase analysis of oxidation and combustion products of stoichiometric mixtures of barium nitrate with aluminum, magnesium and magnalium

Stoichiometric amounts of $Ba(NO_3)_2$/Al, $Ba(NO_3)_2$/Mg and $Ba(NO_3)_2$/AlMg were formed in the form of rods 5 mm in diameter, bound with NC lacquer. At 650°C, the $Ba(NO_3)_2$/Al and $Ba(NO_3)_2$/Mg rods ignited rather quickly and burned out in a few seconds. $Ba(NO_3)_2$/AlMg rods did not ignite when gradually heated to 650°C, but when quickly introduced into the furnace at that temperature they became red hot and quickly ignited. To obtain combustion products, samples were burned in a fume hood under a special smoke-capturing device constructed with quartz tube, from which solid products were extracted and analyzed. Oxidation products for $Ba(NO_3)_2$/Al and $Ba(NO_3)_2$/Mg were obtained at a temperature that was sufficiently low to prevent ignition from occurring.

Table 2. The results of thermal decomposition and combustion experiments for $Ba(NO_3)_2$/AlMg

No.	Initial composition	Heat treatment	Identified phases by XRD
1.	$Ba(NO_3)_2$/AlMg	800°C/30sec	$Ba(NO_3)_2$, $BaCO_3$, AlMg, Al, MgO, Unidentified products (small amount)
		650°C/10min	$Ba(NO_3)_2$, $BaCO_3$, AlMg, Al, MgO, Unidentified products (traces)
		650°C/30min	$Ba(NO_3)_2$, $BaCO_3$, AlMg, Al, MgO, Unidentified products (small amount)
		650°C/1h	$BaAl_2O_4$, $BaCO_3$, Al, MgO, Unidentified products (moderate amount)
		650°C/3h	$BaAl_2O_4$, $BaCO_3$, Al, MgO, Unidentified products (large amount)
		650°C/24h	$BaAl_2O_4$, $BaCO_3$, Al, MgO, Unidentified products (small amount)
		After DTA/TGA (up to 1000°C)	$BaAl_2O_4$, $BaCO_3$, MgO, $MgAl_2O_4$, Other products (traces) *
		After DTA/TGA (up to 1200°C)	$BaAl_2O_4$, MgO, $MgAl_2O_4$
2.	$Ba(NO_3)_2$/AlMg/ Bi_2O_3/NC	Smoke / Ash	$BaAl_2O_4$, MgO, Bi, Other products (traces) **

** $Ba_3Al_2O_6$ ($3BaO{\cdot}Al_2O_3$), $Ba_4Al_2O_7$ ($4BaO{\cdot}Al_2O_3$). ** $BaMgO_2$, $Ba_3Al_2O_6$ ($3BaO{\cdot}Al_2O_3$).*

Phase analysis of oxidation and combustion products of $Ba(NO_3)_2$/Mg

The $Ba(NO_3)_2$/Mg samples oxidized slowly and did not ignite at temperatures not exceeding 500°C. After heating at 500°C for 5 hours, a sample was found to contain $Ba(NO_3)_2$, $BaCO_3$, MgO and Mg, with the oxidation reaction being 64% complete. Above 500°C, a sample burned quickly, leaving almost no ash. The diffractograms of ash and collected solid smoke are presented in Figure 11. As expected, the combustion products were MgO and BaO, the latter absorbing CO_2 to form $BaCO_3$.

Phase analysis of oxidation and combustion products of $Ba(NO_3)_2$/Al

$Ba(NO_3)_2$/Al samples were gradually heated from 500 to 600°C and held at that temperature for a certain time, while the change in weight was recorded. According to the reaction $3Ba(NO_3)_2 + 10Al = 3BaO + 5Al_2O_3 + 3N_2$, the weight loss should be 8%, but if the aluminum does not oxidize or otherwise react with barium nitrate, the weight loss would be 31%. The observed weight loss was found to be 23%, which indicated a partial oxidation process. X-ray phase analysis partially confirmed this. The diffractogram could not be fully refined due to the presence of additional peaks of an unknown phase. Accurately determined compounds were $BaCO_3$, $BaAl_2O_4$ and Al. As illustrated in Figure 12, the smoke from fully combusted $Ba(NO_3)_2$/Al samples was almost free of any unknown compounds. It is interesting to note that the presence of small amounts of $BaCO_3$ and Al in the collected smoke indicates the partial dispersion of the initial components during the combustion of the mixture.

Phase analysis of oxidation and combustion products of $Ba(NO_3)_2$/AlMg

Pressed $Ba(NO_3)_2$/AlMg pellets without any additives or binders were used to study the decomposition products formed during slow oxidation and to obtain DTA/TGA curves. Since the $Ba(NO_3)_2$/AlMg samples consolidated with NC lacquer were difficult to ignite, up to 3% Bi_2O_3 was added, which made them easier to ignite and to burn in a relatively stable and continuous manner, with the production of a sufficient amount of smoke. The results of the thermal decomposition and combustion experiments are presented in Table 2. X-ray diffraction pattern of the combustion products is given in Figure 13.

During heat treatment of $Ba(NO_3)_2$/AlMg at a temperature of 650°C over different time intervals, we observed the following:

1. Up to an hour, partial decomposition of $Ba(NO_3)_2$ and partial oxidation of AlMg.

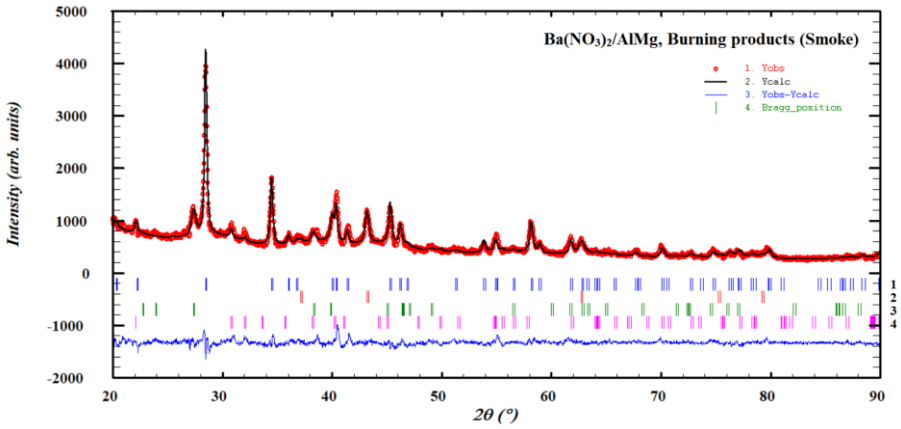

Figure 13. Refined powder X-ray diffraction patterns for the combustion products of $Ba(NO_3)_2$/AlMg (1 - $BaAl_2O_4$, 2 - MgO, 3 - Bi, 4 – $BaMgO_2$; R_p = 5.28%, R_{wp} = 6.86%).

2. Between an hour and 24 hours, $Ba(NO_3)_2$ completely decomposes, magnesium in the AlMg alloy is completely oxidized to MgO, and part of the aluminum to Al_2O_3, which reacts with BaO to form $BaAl_2O_4$. In the same interval, we identify the formation of different amounts of unknown compounds (additional new reflections in the XRD patterns) that are possibly new and/or metastable ones with one or more elements in the Ba-Al-O, Ba-Mg-O or Ba-Al-Mg-O systems. It is possible that they are also the result of the interaction of starting and intermediate products with moisture and/or CO_2.
3. When $Ba(NO_3)_2$/AlMg is heated at a temperature of 650°C for 24 hours and above, these unknown phases almost completely disappear. They were also not detected in samples heated to higher temperatures, in particular, in products after DTA/TGA analyses that raised the temperature above 1000°C. It is planned to continue this work on phase identification and to establish the crystal structure of potential new intermediate phases.

In the collected smoke from the combustion of $Ba(NO_3)_2$/AlMg/Bi_2O_3/NC, two major products, $BaAl_2O_4$ and MgO, were found, corresponding to the combustion reaction: $Ba(NO_3)_2 + 2AlMg = BaAl_2O_4 + 2MgO + N_2$. Metallic bismuth was also detected in the products, which could be formed by the reaction $Bi_2O_3 + 3Mg = 2Bi + 3MgO$. Additional low intensity reflections that were detected on the XRD pattern may belong to other barium compounds, for example, $Ba_3Al_2O_6$ and/or $BaMgO_2$.

We performed DTA/TGA analysis twice, up to temperatures of 1000 and 1200°C for

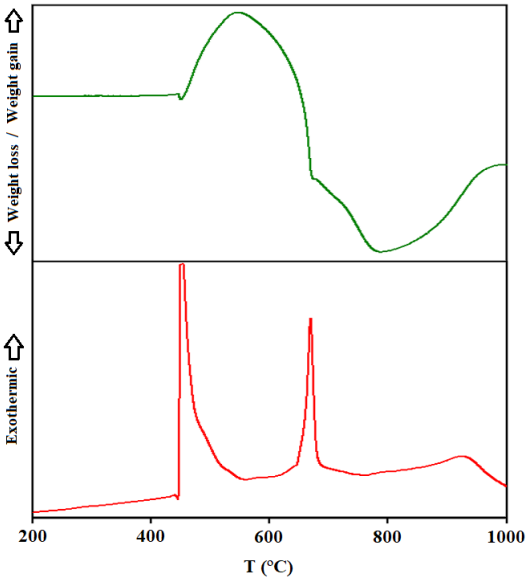

Figure 14. DTA/TGA curves for $Ba(NO_3)_2$/AlMg at a heating rate of 10°C/min in air.

$Ba(NO_3)_2$/AlMg without any additives or binders. As can be seen from the example curves shown in Figure 14, no clear effects were visible at temperatures below about 420 to 440°C. Above 440°C, a strong exothermic peak on the DTA curve and an increase in weight on the TGA curve were observed. It is assumed that as soon as magnalium becomes liquid above 440°C, a significant part of magnesium begins to oxidize rapidly and, according to TGA, the weight continues to increase until the temperature rises to around 540 to 550°C. The first maximum on the DTA curve approximately corresponds to this point. The characteristic convexity on the right side of the TGA peak may correspond to the release of pure magnesium and its oxidation according to the stepwise scheme: $8AlMg + 3O_2 = 6MgO + 2Al_4Mg$, followed by $2Al_4Mg + O_2 = 2MgO + 8Al$. Here, for

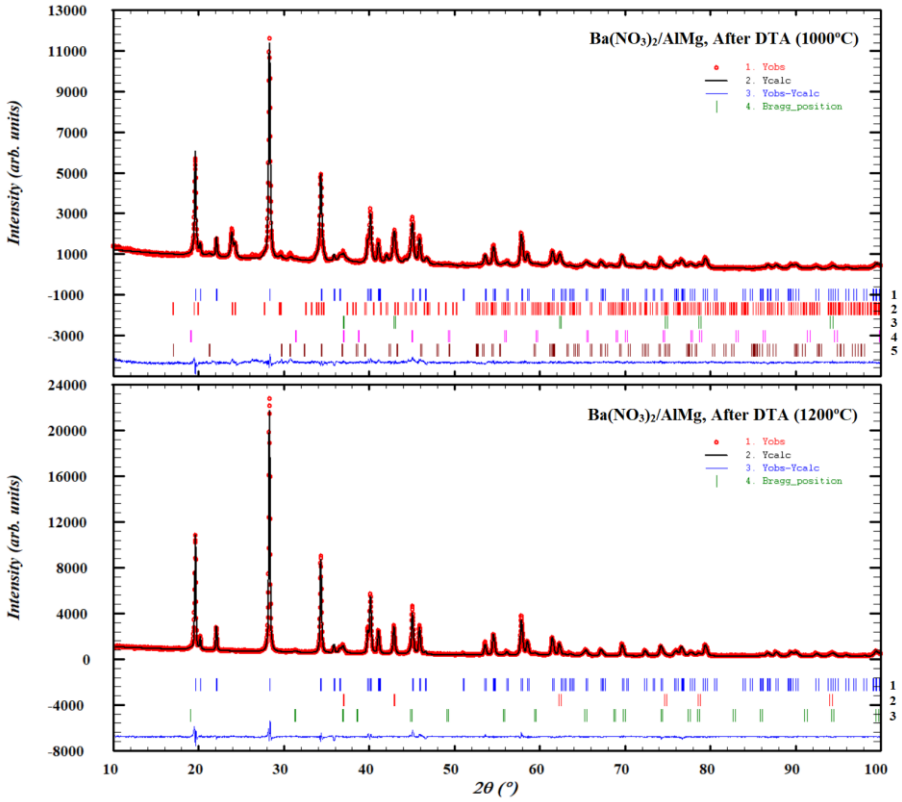

Figure 15. Refined powder X-ray diffraction patterns for the products of $Ba(NO_3)_2$/AlMg after DTA/TGA up to 1000 and 1200°C: (*a*) (1 - $BaAl_2O_4$, 2 - $BaCO_3$, 3 - MgO, 4 - $MgAl_2O_4$, 5 - $BaMgO_2$; R_p = 4.03%, R_{wp} = 5.17%) and (*b*) (1 - $BaAl_2O_4$, 2 - MgO, 3 - $MgAl_2O_4$; R_p = 4.42%, R_{wp} = 6.02%).

convenience, we have chosen Al_4Mg as the intermediate product because it is, according to the Al-Mg phase diagram, the alloy with the maximum solubility of magnesium in aluminum. The increase in weight up to 550°C is lower than the theoretical value for the full transformation of magnesium to MgO. Thus only about 60% of magnesium was oxidized at this stage.

Above the temperature of 550°C, a sharp decrease in weight on the TGA curve was detected, which slows down around the temperature of 670°C, i.e. slightly above the melting point of pure aluminum, at 660°C, and ends at a temperature of about 780°C. The sharp loss of weight is due to the decomposition of barium nitrate, which begins above 550°C. Our results indicate neither the nature of the final decomposition products nor the temperature at which they appear. In consequence, we can do no more than propose a general form for the decomposition reaction: $2Ba(NO_3)_2 = 2BaO + 4NO_x + (5\text{-}2x)O_2$ (x = 0, 1, 2). The decomposition of barium nitrate can also occur in a stepwise fashion.

The DTA analysis shows a second exothermic peak at 670°C. If it is assumed that all the magnesium was oxidized by the time the temperature reached this value, then this second peak is likely to be the result of the oxidation of aluminum. Above 660°C, metallic aluminum melts, and liquid aluminum oxidizes more easily ($4Al + 3O_2 = 2Al_2O_3$). The variations in the rate of weight loss in the range from 670 to 780°C are likely to be the consequence of two overlapping processes; a decrease in weight resulting from the decomposition of barium nitrate and an increase caused by the continuing oxidation of aluminum. Two zones with different rates of weight loss can be seen. It should be noted that, in the presence of Al_2O_3 as a catalyst, the formation of barium peroxide ($BaO + NO_2 = BaO_2 + NO$ and/or $2BaO + O_2 = 2BaO_2$) – or other products resulting from the partial decomposition of barium nitrate – is possible. The minimum on the TGA curve is at 780°C, which probably indicates the completion of the decomposition of barium nitrate. Above this temperature, the remaining aluminum (about 40% according TGA) continues to oxidize and the weight of the sample increases. The DTA curve shows a broad third

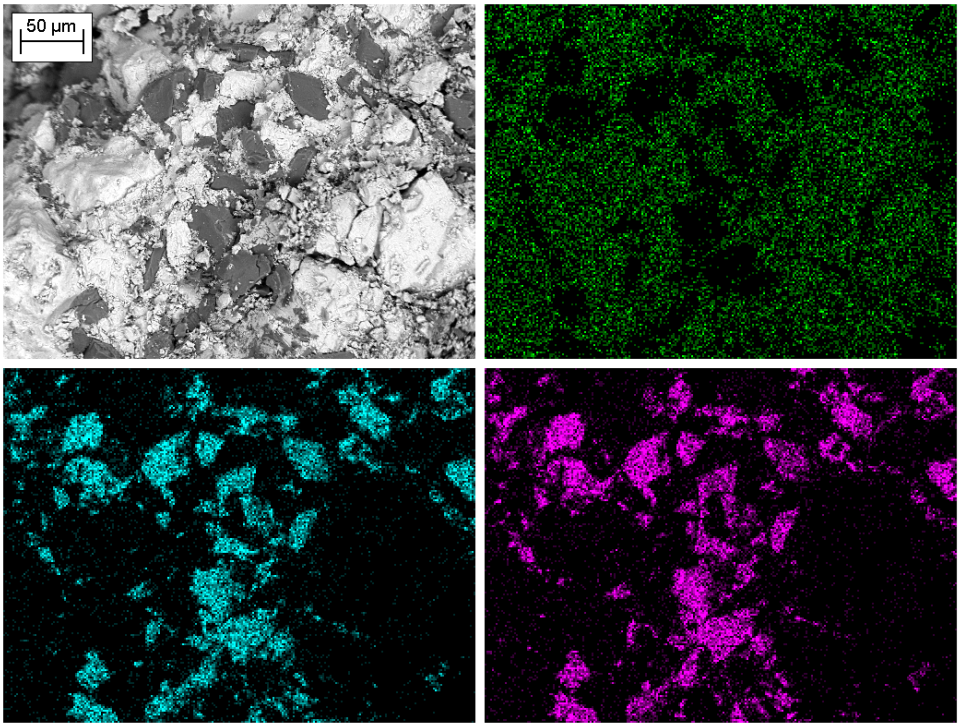

Figure 16. Microphotograph of the surface of the pressed $Ba(NO_3)_2$/AlMg pellet and the elemental distribution of barium (green), magnesium (blue) and aluminum (purple).

exothermic peak at 900 to 910°C that could be the result of the formation of barium aluminate: $BaO + Al_2O_3 = BaAl_2O_4$. The TGA curve shows that the weight stops increasing when the temperature reaches 1000°C.

The chemical processes described here are somewhat idealized. The product samples used in the DTA/TGA analysis were subsequently analyzed by X-ray diffraction, with the results shown in Figure 15. Although trace amounts of $MgAl_2O_4$, $Ba_3Al_2O_6$ and/or $Ba_4Al_2O_7$ were detected in the reaction products, the overall process can be summarized as follows: $Ba(NO_3)_2 + 2AlMg = BaAl_2O_4 + 2MgO + N_2$.

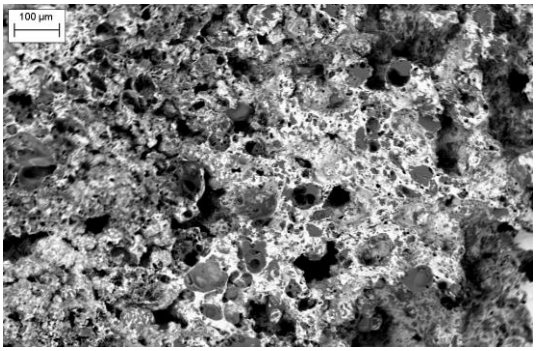

Figure 17. Microstructure of the longitudinal fracture of strobe foam.

Microstructural studies of $Ba(NO_3)_2$/AlMg

Figure 16 shows a microphotograph of the surface of a pressed $Ba(NO_3)_2$/AlMg pellet, together with colored images that reveal the elemental distribution of barium, magnesium and aluminum. In the first image, barium nitrate particles are represented in white,

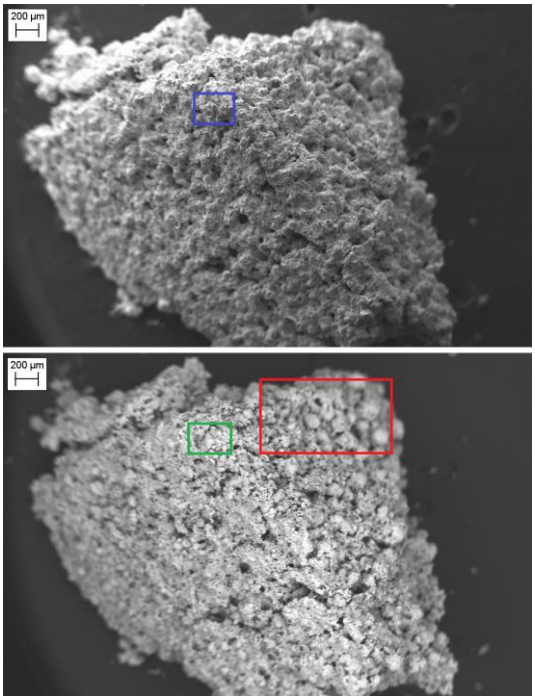

Figure 18. SEM images of the surface of a foam sample, using SE (top) and BSD (bottom) techniques.

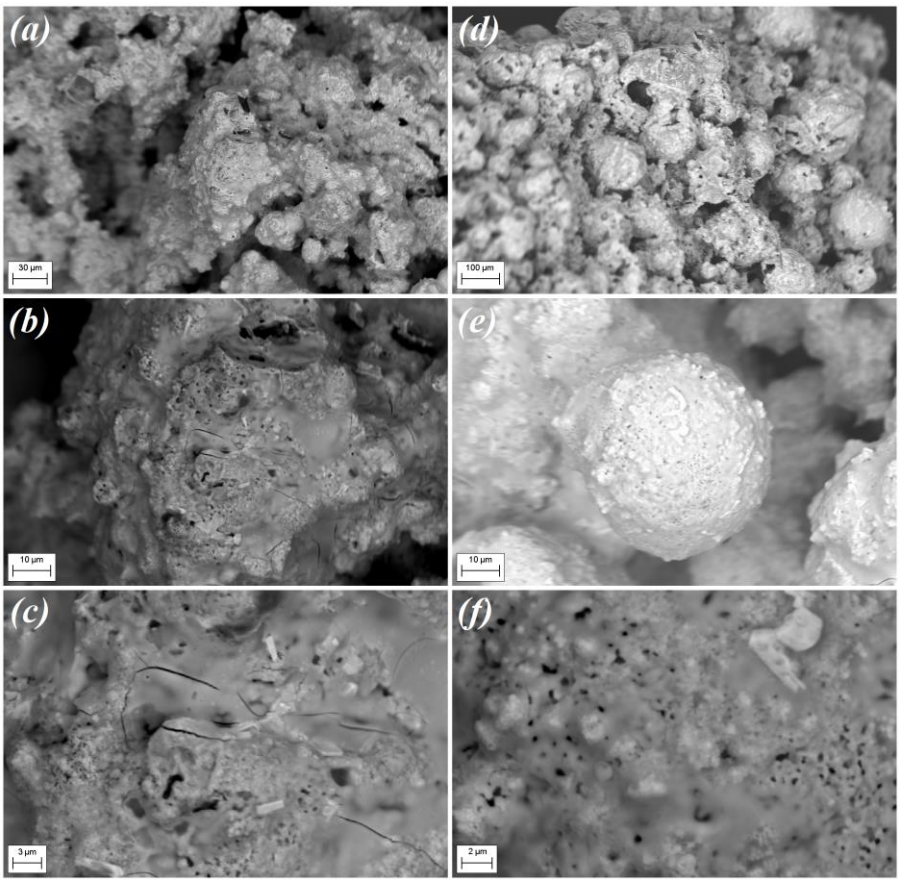

Figure 19. Magnifications of selected areas of strobe foam, from within the regions that are outlined in Figure 18 by the green (a, b, c), red (d) and blue (e, f) rectangles.

while the granular magnalium alloy is seen in dark gray.

It is known that the burning of the strobes is accompanied by the formation of porous foam. The morphology of a sample of the foam, which was formed at 650°C before ignition on a pressed $Ba(NO_3)_2$/AlMg pellet, was studied at different magnifications and the chemical composition of its various areas were established with the aid of an electron microscope. The microphotograph in Figure 17 is an image of the fracture at the interface of the foam and the unreacted mixture and shows the presence of numerous pores. The barium nitrate had fused and begun to decompose. Magnalium also melted, its granules became rounded in shape, many of them pitted with holes that may evidence the partial evaporation of magnesium. The distribution of magnesium and aluminum in these particles is close to 1:1.

Scanning electron microscope (SEM) images of a particle from the surface of the strobe foam, using both secondary electron (SE) and backscattered electron (BSD) detectors, are shown in Figure 18. The structure of the foam is kidney-shaped with holes and cavities on the surface, and almost perfect spherical-shaped forms can also be found. Their sizes vary between around 50 to 200 µm. Magnified images of these forms from the areas highlighted by the colored rectangles in Figure 18 are presented in Figure 19. Rounded shapes are mostly hollow and are the result of more intensive gas release in this zone.

Table 3. The Ba:Al:Mg atomic count ratios for different strobe foam regions, according to SEM/EDS analysis

Area	Ba	Al	Mg
Blue B1	66	25	9
Blue B2	47	38	15
Blue B3	72	25	3
Blue B4	52	40	8
Blue B5	64	35	1
Green G1	58	28	14
Green G2	63	26	1
Green G3	60	29	1
Red R1	47	41	12
Red R2	40	37	23
Red R3	40	37	23
Spectra A	96	2	2
Spectra B	83	13	4

Spectra A & B – point analysis of the white crystals

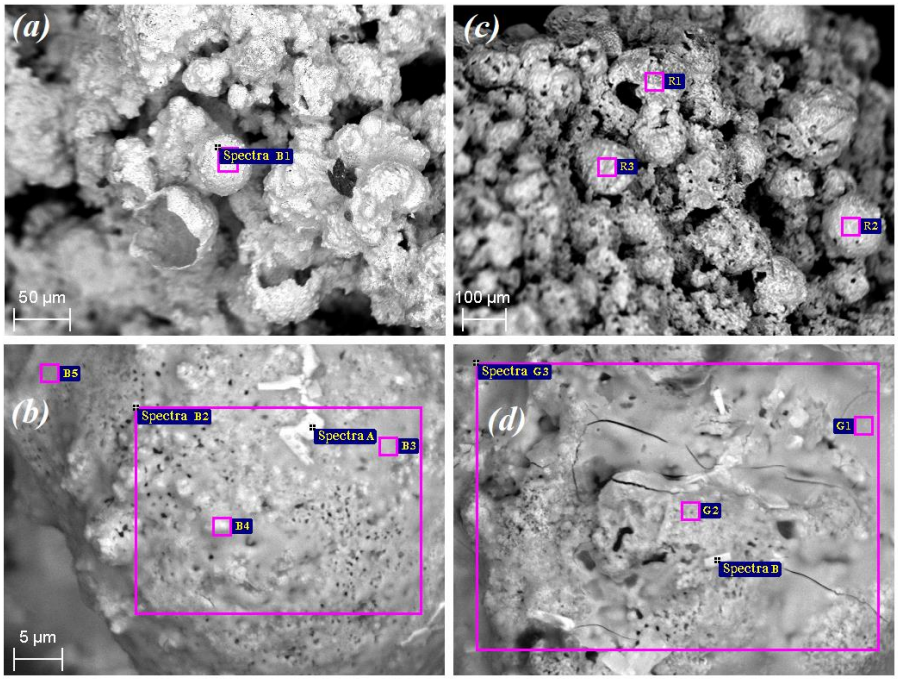

Figure 20. The areas within the blue (a, b), red (c) and green (d) rectangles in Figure 18 that were the subject of EDS analysis.

Kidney-shaped formations consist of layers of partially reacted mixture, alternating with cavities. Both forms, under higher magnification and detailed examination, are riddled with numerous small holes and cracks with sizes up to 1 µm. Crater-like holes up to 30 µm in size can be found on the foam's surface.

Energy dispersive spectroscopy (EDS) techniques were used to provide chemical analyses of both unreacted pellets and the regions of strobe foam shown in Figure 20, which include examples of both spherical and kidney shaped structures. In all cases, the calculation ignored the content of lighter atoms (C, N, O) whose presence may possibly be the result of the surface absorption of atmospheric CO_2, N_2, O_2 and moisture. As expected, the analysis of the unreacted pellets gave an atomic Ba:Al:Mg ratio of 20:40:40, consistent with the content of a stoichiometric mixture of $Ba(NO_3)_2$ and magnalium. The results of the analysis for the eleven regions indicated in Figure 20 are listed in Table 3, showing that the Ba:Al:Mg ratio varies significantly across the samples' surfaces. However, one significant feature is that, with measured values ranging from 1 to 23%, all the results show a marked reduction in the proportion of magnesium. This may be explained by noting that the vapor pressure of magnesium at 650°C is eight orders of magnitude higher than that of aluminum [65, 66]. Its high volatility at such temperatures means that it might easily diffuse from the surface (and subsequently oxidize in the surrounding air), thereby resulting in the observed low content on the surface of the studied strobe foam.

Conclusions

The phase composition of oxidation and combustion products of aluminum, magnesium, and magnalium powders and their stoichiometric mixtures with barium nitrate was studied by using X-ray diffraction analysis. Powdered magnesium oxidizes and burns easily, either alone or when combined with barium nitrate. Aluminum, even in the form of powder, is more resistant to oxidation. When it is mixed with barium nitrate, $BaAl_2O_4$ is formed in both oxidation and combustion products. Oxidation of metal powders under an oxygen deficiency can lead to the formation of the corresponding nitrides, Mg_3N_2 or AlN. Magnalium and its mixture with barium nitrate show at least two-stage oxidation behavior, which was deduced from the results of XRD, DTA/TGA, SEM/EDS analyses. This observation may be the key to understanding the combustion of strobe pyrotechnic mixtures. A stoichiometric mixture of barium nitrate and magnalium is difficult to ignite; it burns in an unstable

manner and tends to self-extinguish. Catalysts such as bismuth oxide, the role of which still needs to be clarified, can drastically modify the burning characteristics of $Ba(NO_3)_2$/AlMg mixtures.

Acknowledgements

I am grateful to Richard Harrison for his constructive and helpful preliminary review and edit of this paper.

References

1 Y. Verbovytskyy, R. Harrison, Pyrotechnic strobe compositions: an overview, *Propellants, Explosives, Pyrotechnics,* Vol. 47, 2022, e202100311, pp. 1-11

2 T. Shimizu, Studies on strobe light pyrotechnic compositions, *Pyrotechnica,* Vol. 8, 1982, pp. 5-34

3 C. Jennings-White, Strobe chemistry, *Journal of Pyrotechnics,* Vol. 20, 2004, pp. 7-16.

4 E.L. Charsley, P.G. Laye, M.E. Brown, Pyrotechnics, *Handbook of Thermal Analysis and Calorimetry,* Vol. 2, 2003, pp. 777-815

5 D. Barisin, I. Batinic-Haberle, Aging of pyrotechnic compositions. The investigation of chemical changes by IR spectroscopy and X-ray diffraction, *Propellants, Explosives, Pyrotechnics,* Vol. 14, 1989, pp. 162-169

6 V. Khire, N. M. Bhide, E. M. Kurian, Thermal, combustion and luminosity studies on magnesium - strontium nitrate pyrotechnic system, *Journal of Energetic Materials,* Vol. 16, 1998, pp. 45-68

7 I. Tuukkanen, S. D. Brown, E. L. Charsley, S. J. Goodall, J. J. Rooney, T. T. Griffiths, H. Lemmetyinen, Studies on the ageing of a magnesium - strontium nitrate pyrotechnic composition using isothermal microcalorimetry and thermal analysis techniques, *Thermochimica Acta,* Vol. 417, 2004, pp. 223-229

8 I. M. Tuukkanen, S. D. Brown, E. L. Charsley, S. J. Goodall, P. G. Laye, J. J. Rooney, T. T. Griffiths, H. Lemmetyinen, A study of the influence of the fuel to oxidant ratio on the ageing of magnesium - strontium nitrate pyrotechnic compositions using isothermal microcalorimetry and thermal analysis techniques, *Thermochimica Acta,* Vol. 426, 2005, pp. 115-121

9 I. M. Tuukkanen, E. L. Charsley, S. J. Goodall, P. G. Laye, J. J. Rooney, T. T. Griffiths, H. Lemmetyinen, An investigation of strontium nitrite and its role in the ageing of the magnesium - strontium nitrate pyrotechnic system using isothermal microcalorimetry and thermal analysis techniques, *Thermochimica Acta,* Vol. 443, 2006, pp. 116-121

10 I. M. Tuukkanen, E. L. Charsley, P. G. Laye, J. J. Rooney, T. T. Griffiths, H. Lemmetyinen, Pyrotechnic and thermal studies on the magnesium - strontium nitrate pyrotechnic system, *Propellants, Explosives, Pyrotechnics,* Vol. 31, 2006, pp. 110-115

11 P. J. Disimile, R. Prasad, N. Toy, Temperature measurements within the luminous region of a burning $Ba(NO_3)_2$/Al mixture, *Journal of Pyrotechnics,* Vol. 23, 2006, pp. 10-20

12 M. Yao, L. Chen, J. Yu, J. Peng, Thermoanalytical investigation on pyrotechnic mixtures containing Mg-Al alloy powder and barium nitrate, *Procedia Engineering,* Vol. 45, 2012, pp. 567-573

13 D. Ouyang, Effect of different binders on the combustion characteristics of $Ba(NO_3)_2$/Mg-containing pyrotechnic mixtures, *Central European Journal of Energetic Materials,* Vol. 10, 2013, pp. 209-215

14 C. Zhu, H. Wang, L. Min, Ignition temperature of magnesium powder and pyrotechnic composition, *Journal of Energetic Materials,* Vol. 32, 2014, pp. 219-226

15 Z. Babar, A. Q. Malik, Thermal decomposition, ignition and kinetic evaluation of magnesium and aluminium fuelled pyrotechnic compositions, *Central European Journal of Energetic Materials,* Vol. 12, 2015, pp. 579-592

16 X. Chen, D. Ouyang, Q. Zhang, Comparative study of the combustion characteristics for modified barium nitrate and ordinary barium nitrate, *Science and Technology of Energetic Materials,* Vol. 78, 2017, pp. 1-4

17 H. R. Pouretedal, S. L. Mousavi, Study of the ratio of fuel to oxidant on the kinetic

of ignition reaction of Mg/$Ba(NO_3)_2$ and Mg/$Sr(NO_3)_2$ pyrotechnics by non-isothermal TG/DSC technique, *Journal of Thermal Analysis and Calorimetry,* Vol. 132, 2018, pp. 1307-1315
18 A. Jain, S. P. Ong, G. Hautier, W. Chen, W. D. Richards, S. Dacek, S. Cholia, D. Gunter, D. Skinner, G. Ceder, K. A. Persson, Commentary: The Materials Project: A materials genome approach to accelerating materials innovation, *APL Materials,* Vol. 1, 2013, 011002, pp. 1-11
19 W. Kraus, G. Nolze, POWDER CELL - a program for the representation and manipulation of crystal structures and calculation of the resulting X-ray powder patterns, *Journal of Applied Crystallography,* Vol. 29, 1996, pp. 301-303
20 J. Rodríguez-Carvajal, Recent developments of the program FULLPROF, Commission on Powder Diffraction (IUCr), *Newsletter,* Vol. 26, 2001, pp. 12-19
21 Y. Verbovytskyy, On barium nitrate - magnalium-based strobes, *American Fireworks News,* Vol. 491, 2022, pp. 1-4
22 X. Zhang, X. Chen, M. Feng, Z. Zheng, G. Pan, H. Lv, Influences of bulking and porous structure on barium nitrate as pyrotechnic oxidants, *Advanced Materials Research,* Vol. 550-553, 2012, pp. 27-31
23 V. D. Hogan, S. Gordon, A thermoanalytical study of the binary oxidant system potassium perchlorate-barium nitrate, *The Journal of Physical Chemistry,* Vol. 62, 1958, pp. 1433-1435
24 X. Chen, X. Zhang, M. Feng, G. Pan, H. Lv, The influences of catalysts in the thermal decomposition of barium nitrate as pyrotechnic oxidants, *Applied Mechanics and Materials,* Vol. 217-219, 2012, pp. 766-769
25 Z. Babar, A. Q. Malik, Synthesis of micro porous barium nitrate with improved ignition reliability as a reliable pyrotechnic oxidant, *Journal of Saudi Chemical Society,* Vol. 18, 2014, pp. 707-711
26 C. J. Bardwell, R. I. Bickley, S. Poulston, M. V. Twigg, Thermal decomposition of bulk and supported barium nitrate, *Thermochimica Acta,* Vol. 613, 2015, pp. 94-99
27 S. S. Devi, G. Rajashekhar, S. N. Reddy, A. S. Chary, Characterization of $Ba(NO_3)_2$ and KNO_3 and their composite systems through SEM and DSC, *AIP Conference Proceedings,* Vol. 2269, 2020, 030065, pp. 1-5
28 D. Ouyang, Q. Zhang, X. Chen, Z. Guo, C. Yang, Preparation and the thermal properties of porous barium nitrate, *Science and Technology of Energetic Materials,* Vol. 82, 2021, pp. 89-94
29 J. L. Murray, The Al-Mg (Aluminum - Magnesium) system, *Bulletin of Alloy Phase Diagrams,* Vol. 3, 1982, pp. 60-65
30 P. P. Schobinger, P. Fischer, Neutronenbeugungsuntersuchung der Atom-verteilung von $Mg_{17}Al_{12}$, *Naturwissenschaften,* Vol. 57, 1970, pp. 128-129
31 M. Feuerbacher, C. Thomas, J. P. A. Makongo, The Samson phase, β-Mg_2Al_3, revisited, *Zeitschrift für Kristallographie,* Vol. 222, 2007, pp. 259-288
32 H. L. Su, M. Harmelin, P. Donnadieu, C. Baetzner, H. J. Seifert, H. L. Lukas, G. Effenberg, F. Aldinger, Experimental investigation of the Mg-Al phase diagram from 47 to 63 at.% Al, *Journal of Alloys and Compounds,* Vol. 247, 1997, pp. 57-65
33 P. Liang, H. L. Su, P. Donnadieu, M. G. Harmelin, A. Quivy, P. Ochin, G. Effenberg, H. J. Seifert, H. L. Lukas, F. Aldinger, Experimental investigation and thermodynamic calculation of the central part of the Mg-Al phase diagram, *Zeitschrift für Metallkunde,* Vol. 89, 1998, pp. 536-540
34 K. F. Kobayashi, T. Awazu, P. H. Shingu, New metastable phases in the Al-Mg system, *Journal of Materials Science Letters,* Vol. 6, 1987, pp. 781-783
35 A. Calka, W. Kaczmarek, J. S. Williams, Extended solid solubility in ball-milled Al-Mg alloys, *Journal of Materials Science,* Vol. 28, 1993, pp. 15-18
36 V. Fournée, E. Belin-Ferré, A. Sadoc, P. Donnadieu, A. M. Flank, H. Müller, Atomic and electronic structure of quasiperiodic and crystalline Mg-61 at.% Al alloys, *Journal of Physics: Condensed Matter,* Vol. 11, 1999, pp. 191-208
37 P. Donnadieu, M. G. Harmelin, H. J. Seifert, F. Aldinger, Commensurately modulated stable states related to the γ phase in Mg-Al alloys, *Philosophical Magazine A,* Vol. 78, 1998, pp. 893-905

38 M. Schoenitz, E. Dreizin, Oxidation processes and phase changes in metastable Al-Mg alloys, *Journal of Propulsion and Power,* Vol. 20, 2004, pp. 1064-1068
39 Y. Aly, M. Schoenitz, E. L. Dreizin, Ignition and combustion of mechanically alloyed Al-Mg powders with customized particle sizes, *Combustion and Flame,* Vol. 160, 2013, pp. 835-842
40 H.-T. Huang, M.-S. Zou, X.-Y. Guo, R.-J. Yang, Y.-K. Li, E.-Z. Jiang, Z.-S. Li, Study of different Al/Mg powders in hydroreactive fuel propellant used for water ramjet, *Journal of Energetic Materials,* Vol. 32, 2014, pp. S83-S93
41 H. Zou, L. Li, S. Cai, Effect of magnesium-rich phase on oxidation properties of atomized aluminum - magnesium powders, *Journal of Propulsion and Power,* Vol. 32, 2016, pp. 1-6
42 H. Nie, M. Schoenitz, E. L. Dreizin, Oxidation of differently prepared Al-Mg alloy powders in oxygen, *Journal of Alloys and Compounds,* Vol. 685, 2016, pp. 402-410
43 H. Belal, C. W. Han, I. E. Gunduz, V. Ortalan, S. F. Son, Ignition and combustion behavior of mechanically activated Al-Mg particles in composite solid propellants, *Combustion and Flame,* Vol. 194, 2018, pp. 410-418
44 X. Xie, C.-G. Yan, Y.-K. Wang, J.-R. Xu, C.-G. Zhu, Preparation of aluminum nitride by combustion of a Mg-Al alloy, *Ceramics International,* Vol. 45, 2019, pp. 18721-18726
45 X. Huang, Y. Yang, F. Hou, S. Li, Z. Qin, F. Zhao, Laser-induced ignition and combustion of Al-Mg alloy powder prepared by melt atomization, *Propellants, Explosives, Pyrotechnics,* Vol. 45, 2020, pp. 1645-1653
46 Y.-K. Wang, X. Xie, C.-G. Zhu, Self-propagating high-temperature synthesis of magnesium aluminate spinel using Mg-Al Alloy, *ACS Omega,* Vol. 7, 2022, pp. 12617-12623
47 H. Nie, M. Schoenitz, E.L. Dreizin, Oxidation of magnesium: implication for aging and ignition, *The Journal of Physical Chemistry C,* Vol. 120, 2016, pp. 974-983
48 G. Moser, V. Tschamber, C. Schonnenbeck, A. Brillard, J.-F. Brilhac, Non-isothermal oxidation and kinetic analysis of pure magnesium powder, *Journal of Thermal Analysis and Calorimetry,* Vol. 136, 2019, pp. 2145-2155
49 M. Karimpour, S. R. Eatezadi, S. Hasani, A. Ghaei, The oxidation mechanism of pure magnesium powder particles: A mathematical approach, *Metallurgical and Materials Transactions B,* Vol. 50, 2019, pp. 1597-1607
50 G. Moser, C. Schonnenbeck, V. Tschamber, A. Brillard, J.-F. Brilhac, Experimentation and kinetic modeling of low-temperature oxidation of magnesium particles for the production of energy with low environmental impact, *Combustion and Flame,* Vol. 230, 2021, 111419, pp. 1-10
51 Y. Li, J. Wang, D. Shen, H. Liu, D. Song, Y. Li, Reactions and Morphologies of Mg and Mg/Teflon/Viton Particles during Oxidation, *Metals,* Vol. 13, 2023, 417, pp. 1-14
52 F. Zong, C. Meng, Z. Guo, F. Ji, H. Xiao, X. Zhang, J. Ma, H. Ma, Synthesis and characterization of magnesium nitride powder formed by Mg direct reaction with N_2, *Journal of Alloys and Compounds,* Vol. 508, 2010, pp. 172-176
53 Q. S. M. Kwok, R. C. Fouchard, A.-M. Turcotte, P. D. Lightfoot, R. Bowes, D. E. G. Jones, Characterization of aluminum nanopowder compositions, *Propellants, Explosives, Pyrotechnics,* Vol. 27, 2002, pp. 229-240
54 N. Eisenreich, H. Fietzek, M. M. Juez-Lorenzo, V. Kolarik, A. Koleczko, V. Weiser, On the mechanism of low temperature oxidation for aluminum particles down to the nano-scale, *Propellants, Explosives, Pyrotechnics,* Vol. 29, 2004, pp. 137-145
55 M. A. Trunov, M. Schoenitz, X. Zhu, E. L. Dreizin, Effect of polymorphic phase transformations in Al_2O_3 film on oxidation kinetics of aluminum powders, *Combustion and Flame,* Vol. 140, 2005, pp. 310-318
56 S. Hasani, M. Panjepour, M. Shamanian, The oxidation mechanism of pure aluminum powder particles, *Oxidation of Metals,* Vol. 78, 2012, pp. 179-195
57 K. Wefers, C. Misra, Oxides and hydroxides of aluminum. ALCOA.

Laboratories-Aluminum Company of America, Paper No. 19, 1987
58 I. Levin, D. Brandon, Metastable alumina polymorphs: Crystal structures and transition sequences, *Journal of the American Ceramic Society,* Vol. 81, 1998, pp. 1995-2012
59 M. A. Trunov, M. Schoenitz, E. L. Dreizin, Effect of polymorphic phase transformations in alumina layer on ignition of aluminium particles, *Combustion Theory and Modelling,* Vol. 10, 2006, pp. 603-623
60 M. A. Trunov, M. Schoenitz, E. L. Dreizin, Ignition of aluminum powders under different experimental conditions, *Propellants, Explosives, Pyrotechnics,* Vol. 30, 2005, pp. 36-43
61 A. Gromov, V. Vereshchagin, Study of aluminum nitride formation by superfine aluminum powder combustion in air, *Journal of the European Ceramic Society,* Vol. 24, 2004, pp. 2879-2884
62 M. Vlasova, N. Kakazey, I. Rosales, L. Krushinskaya, A. Bykov, T. Tomila, E. Voitsehovskaya, V. Vinokurov, Synthesis of composite AlN-AlON-Al_2O_3 powders and ceramics prepared by high-pressure sintering, *Science of Sintering,* Vol. 42, 2010, pp. 283-295
63 G. Paglia, Determination of the structure of γ-alumina using empirical and first principles calculations combined with supporting experiments, *Doctoral Thesis, Curtin University of Technology,* 2004
64 M. A. Trunov, Effect of polymorphic phase transformations within an alumina layer on the ignition of aluminum particles, *Doctoral Thesis, New Jersey Institute of Technology,* 2006
65 F. Czerwinski, Oxidation characteristics of magnesium alloys, *The Journal of The Minerals, Metals & Materials Society,* Vol. 64, 2012, pp. 1477-1483
66 D.H. Han, J. Zhang, J. Huang, Y. Lian, G. He, A review on ignition mechanisms and characteristics of magnesium alloys, Journal of Magnesium and Alloys, Vol. 8, 2020, pp. 329-344